

Numerical Study for MHD Flow of an Oldroyd-B Fluid Over a Stretching Sheet in the Presence of Thermal Radiation with Soret and Dufour Effects

Abdelmgid O.M. Sidahmed*

*Department of Mathematics, College of Science & Arts, King Abdulaziz University, Rabigh 21911,
Saudi Arabia*

**Corresponding author: aoahmad2@kau.edu.sa*

ABSTRACT. This paper investigates the impact of Soret and Dufour's MHD flow of an Oldroyd-B fluid over a stretching sheet in the presence of thermal radiation. By a similarity transformation, the controlling partial differential equations are transformed into a system of nonlinear ordinary differential equations. Using the successive linearization method (SLM), the linear system is solved. A determination and discussion of the impacts of specific fluid parameters on the temperature, concentration distribution, and velocity are presented. As the magnetic field increases, we observe that the temperature and concentration profiles rise, while the velocity profile falls. In addition, increases in the Dufour and Soret levels will also result in an improvement in the temperature and concentration distribution. The validity of the acquired results is tested by comparing them to previously published works, with particular attention paid to the accuracy and convergence of the solution.

1. Introduction

Non-Newtonian fluids have garnered a lot of attention over the past twenty years because of their numerous applications in the engineering and industrial sectors. Numerous fluid models have been proposed in the literature to explain the characteristics of non-Newtonian fluids. The three categories of differential type, rate type, and integral type are used to categorize non-Newtonian materials in general. The Maxwell fluid model represents the most straightforward class of rate-type fluids. The Maxwell fluid is incapable of foretelling the properties of retardation time. Both the relaxation and retardation time characteristics were investigated using an Oldroyd-

Received Nov. 23, 2023

2020 *Mathematics Subject Classification.* 80A20.

Key words and phrases. MHD flow; Oldroyd-B fluid; Soret-Dufour; stretching sheet; SLM.

B fluid model [1]. Prasannakumara et al. [2] investigated the flow of MHD 3D Maxwell nanofluid mixed convection across a bidirectional stretched sheet with nonlinear thermal radiation. They solved coupled ODEs using the RKF45 approach, and the findings showed that nonlinear thermal radiation had a major impact on thermal radiation. Ghachem et al. [3] investigated the MHD free convection in a cubical hollow with a perforated wall. They concluded that more pores have a higher heat-transfer efficiency at higher Rayleigh number values. In their investigation of the chemically reacting fluid flow across a porous stretched surface, Bhuvaneshwari et al. [4] considered MHD double-diffusive mixed convection with convective boundary conditions. They talked about flow, thermal, and solutal field analytical and numerical solutions. The significance of the heat source/sink, gravity modulation, and MHD on the micropolar fluid dynamics across an inclined zone was investigated by Ali et al. [5] using FEM. They concluded that higher amplitude modulation enhances the skin-friction fluctuations and heat gradient. Using the FDM approach, Raizah et al. [6] numerically studied the stable 2D laminar MHD mixed-convective flow in curvilinear enclosures fitted with micropolar nanofluids. According to their findings, the dimensionless viscosity, the Hartmann number, and the location of the heat source all have a major impact on the average Nusselt number. Oldroyd [7] first presented it in 1950. According to the Oldroyd-B model, the fluid's stress tensor can be divided into two components: one that is completely viscous and the other that results from the deformation of elastic molecules in the fluid. The impact of double stratification in the mixed convection flow of an Oldroyd-B fluid with heat radiation and chemical reactions was investigated by Hayat et al. [8]. They observed that for the solutal stratification parameter, the temperature and concentration fields exhibit opposing behavior. Shaqfeh [9] studied the flow instabilities that occur when inertial forces are absent. An analysis of the numerical simulation of viscoelastic liquids based on molecular models was performed by Laso and Ottinger [10]. Sajid *et al.* [11] studied the boundary layer stagnation point flow toward a moving sheet in an Oldroyd-B model. For the distribution of velocities at infinite velocity, they provided numerical solutions.

In the presence of Soret, Dufour, and nanoparticles, an electrically conducting Maxwell fluid in two dimensions that is incompressible was studied by Venkatesh et al. [12] for its properties related to mass and heat transfer across a stretching sheet. The numerical simulation of a three-dimensional Oldroyd-B fluid with time dependency by Motsa *et al.* [13] was presented. Hayat *et al.* [14], in the context of the magnetohydrodynamic flow of an Oldroyd-B fluid, examined the Cattaneo–Christov heat flux in the presence of homogeneous and heterogeneous processes. The references [15–21] provide some current studies on Oldroyd-B fluids.

Density differences brought about by concurrent gradients in temperature, concentration, and material composition in combined heat and mass transfer processes drive the flow. The mass flux that a temperature gradient produces is known as the thermal diffusion (Soret) effect. The

diffusion thermo effect (Dufour) is the term used to describe the energy flux resulting from concentration changes. For example, the separation of isotopes and mixtures of gases with very light and medium molecular weights has been applied to the Soret effect. Numerous real-world applications, including those in chemical engineering and geosciences, involve the Soret and Dufour effects. Venkateswarlu and Satya [22] investigated the effects of joule heating by Soret and Dufour on the MHD stream of a Maxwell fluid on a stretched surface. They observed that the velocity and concentration profiles enlarge with the Soret number. Based on their study of how Soret and Dufour affect the MHD stream of Casson fluid, Hayat et al. [23] found that velocity decreases as the Casson parameter increases. Khan et al. [24] studied the simultaneous properties of Soret and Dufour in an entropy-optimized Reiner–Rivlin fluid flow while taking thermal radiation into account. The Soret and Dufour effects on the free convective flow of Casson fluid over a nonlinearly elongating sheet embedded in a porous medium were studied by Biswal et al. [25]. They observed that the Soret and Dufour effects maintain a surface free of solutal deposits and act as a surface coolant. Recent studies in this field have included the numerous effects listed in references [26–31].

Nonlinear equations may be used to model most cosmic phenomena that we encounter in science, physics, and geometry on a daily basis. Approximate mathematical analytical techniques, including the homotopy analysis method (HAM) created by Liao [32] and the Adomain decomposition method (ADM) developed by Makinde [33], can be used to solve some of these nonlinear equations. Several of these equations can be resolved with the use of standard numerical methods such as the Runge–Kutta, Keller box, and finite difference approaches. Recent research has demonstrated the benefits of the successive linearization method (SLM). Numerous science and engineering nonlinear problems have been solved with this technique. A set of linear differential equations has been derived from the governing nonlinear equations using this method. We used the Chebyshev pseudo-spectral approach to solve linear differential equations with higher-order deformation. The SLM methodology can be applied to highly nonlinear system boundary value problems as an alternative to more traditional numerical methods (see references [34–41]).

The purpose of this work is to obtain numerical solutions for the impact of thermal radiation on the MHD flow of an Oldroyd-B fluid over a stretching sheet with Soret and Dufour effects. The successive linearization method (SLM) yields convergent solutions. A graphic analysis was performed to determine how various parameters behave on the relevant physical quantities.

As far as we are aware, no research has been conducted on the impacts of Soret and Dufour on the MHD flow of an Oldroyd-B fluid flow across a stretching surface. As a result, the mathematical formulation for such flows is included in this article. The successive linearization

method (SLM) is used to compute the nonlinear analysis. The results are also contrasted with the limited solutions found in the current literature. The impact of the relevant parameters is thoroughly examined.

2. Mathematical Formulation

2.1. Governing equations and boundary conditions

Consider a steady incompressible two-dimensional fluid that is flowing through a stretched sheet. The MHD effects are saturated as the sheet expands, with the plane $y = 0$. It is assumed that the flow is constrained to $y > 0$. We should posit the possibility that the sheet is stretched continuously with $u(x) = ax$, where $a > 0$ is constant, and the x -axis is approximated along the stretching surface. The stretched surface is given a magnetic field that is consistently consistent and uniform in a normal direction. Under the constant and boundary layer assumptions, the continuous constitutive equation of the Oldroyd-B fluid and energy equation is presented below [42-44]:

$$\frac{\partial u}{\partial x} + \frac{\partial v}{\partial y} = 0, \quad (1)$$

$$\begin{aligned} u \frac{\partial u}{\partial x} + v \frac{\partial u}{\partial y} + \beta \left(u^2 \frac{\partial^2 u}{\partial x^2} + v^2 \frac{\partial^2 u}{\partial y^2} + 2uv \frac{\partial^2 u}{\partial x \partial y} \right) \\ = v \left[\frac{\partial^2 u}{\partial y^2} + \gamma \left(\frac{\partial}{\partial x} \left(u \frac{\partial^2 u}{\partial y^2} \right) + \frac{\partial u}{\partial y} \frac{\partial^2 v}{\partial y^2} + v \frac{\partial^3 u}{\partial y^3} \right) \right] - \frac{\sigma B_0^2}{\rho} u + \\ g\beta_T(T - T_\infty) + g\beta_c(C - C_\infty), \end{aligned} \quad (2)$$

$$u \frac{\partial T}{\partial x} + v \frac{\partial T}{\partial y} = \frac{1}{c_p} \left(\alpha + \frac{16\sigma^* T_\infty^3}{3k^*} \right) \frac{\partial^2 T}{\partial y^2} + \frac{D_m K_T}{c_s c_p} \frac{\partial^2 C}{\partial y^2}, \quad (3)$$

$$u \frac{\partial C}{\partial x} + v \frac{\partial C}{\partial y} = D_m \frac{\partial^2 C}{\partial y^2} + \frac{D_m K_T}{T_m} \frac{\partial^2 T}{\partial y^2}. \quad (4)$$

The corresponding boundary conditions are

$$\begin{aligned} u = Bx, \quad v = V, \quad T = T_w = T_\infty + ax, \quad C = C_w = C_\infty + bx, \quad \text{at } y = 0, \\ u \rightarrow 0, \quad T \rightarrow T_\infty, \quad C \rightarrow C_\infty, \quad \text{as } y \rightarrow \infty, \end{aligned} \quad (5)$$

where B is a constant; (u, v) are the fluid velocity components in the x and y directions, respectively; (a, b) are the gradients of the ambient temperature and concentration profiles stratification rate, respectively; β is the relaxation time; V is the plate surface; and γ is the retardation time. The variables T , β_T , α , and g represent the temperature, volumetric coefficient of thermal expansion, thermal diffusivity, and gravitational acceleration, respectively. The parameters are as follows: T_m is the mean fluid temperature, k^* is the mean absorption coefficient, σ^* is the Stefan-Boltzmann constant, C is the species concentration, σ is the electrical conductivity, k_T is the thermal diffusion ratio, c_s is the concentration susceptibility, c_p is the specific heat at constant pressure, and ν is the kinematic viscosity. B_0 is a symbol for the externally applied magnetic field in the y direction.

2.2. Similarity transformation

The governing equations (2)-(4) can be converted into a set of nonlinear ordinary differential equations by utilizing the following nondimensional variables ([42-44]):

$$u = \frac{\partial \psi}{\partial y} = Bx f'(\eta), v = \frac{\partial \psi}{\partial x} = -\sqrt{Bv} f(\eta), \eta = \sqrt{\frac{B}{v}} y, \theta(\eta) = \frac{T-T_\infty}{T_w-T_\infty}, \phi(\eta) = \frac{C-C_\infty}{C_w-C_\infty}. \tag{6}$$

$$f'''' + ff'' - f'^2 - Mf' + \beta_1(2ff'f'' - f^2f''') + \beta_2(2f'f''' - f''^2 - ff^{iv}) + Gr\theta + Gc\phi = 0, \tag{7}$$

$$\left(\frac{1}{Pr}\right)\left(1 + \frac{4}{3} Rd\right)\theta'' + f\theta' - f'\theta + Du\phi'' = 0, \tag{8}$$

$$\phi'' + Scf\phi' - Scf'\phi + ScSr\theta'' = 0. \tag{9}$$

Additionally, the boundary conditions are modified to the form

$$f(0) = -fw, \quad f'(0) = 1, \quad f'(\infty) = 0, \tag{10}$$

$$\theta(0) = 1, \quad \theta(\infty) = 0, \tag{11}$$

$$\phi(0) = 1, \quad \phi(\infty) = 0, \tag{12}$$

where $\beta_1(= \beta B)$ and $\beta_2(= \gamma B)$ are the Deborah numbers in terms of the relaxation time and retardation time, respectively; $M(= \frac{\sigma B_0^2}{\rho B})$ is the magnetic parameter (Hartman number); $Pr = \nu/\alpha$ is the Prandtl number; $Sc = (\nu/D_m)$ is the Schmidt number; $Gr = (\frac{g\beta_T(T_w-T_\infty)}{xB^2})$ is the local temperature Grashof number; $G_c = (\frac{g\beta_c(C_w-C_\infty)}{xB^2})$ is the local concentration Grashof number; $Du = \frac{D_m K_T (C_w - C_\infty)}{C_s C_p (T_w - T_\infty)}$ is the Dufour number; $Sr = \frac{D_m K_T (T_w - T_\infty)}{T_m (C_w - C_\infty) \nu}$ is the Soret number; $fw = \frac{\nu}{\sqrt{Bv}}$ is the dimensionless suction velocity; and $Rd = \frac{4\sigma^* T_\infty^3}{k^* k}$ is the radiation number.

3. Numerical Methods

We solve the present problem numerically by using the successive linearization method. The governing nonlinear equations (7)-(9) are turned into a set of linear differential equations by the SLM. These equations can then be solved numerically or analytically.

The system (7)-(9) can be solved according to the SLM approach as [45-48] by assuming the following:

$$f(\eta) = f_i(\eta) + \sum_{n=0}^{i-1} f_n(\eta), \quad \theta(\eta) = \theta_i(\eta) + \sum_{n=0}^{i-1} \theta_n(\eta), \quad \phi(\eta) = \phi_i(\eta) + \sum_{n=0}^{i-1} \phi_n(\eta). \tag{13}$$

Starting from an initial guess that is appropriate for $f_0(\eta)$, $\theta_0(\eta)$, and $\phi_0(\eta)$ and that satisfies the boundary conditions (10), (11), and (12), the suitable functions are as follows:

$$f_0(\eta) = 1 - e^{-\eta}, \quad \theta_0(\eta) = e^{-\eta}, \quad \phi_0(\eta) = e^{-\eta}. \tag{14}$$

Substituting equation (13) into the controlling equations (7)-(9), while neglecting the nonlinear terms in $f_i(\eta)$, $\theta_i(\eta)$, $\phi_i(\eta)$, and their derivatives, yields

$$a_1 f_i^{iv} + a_2 f_i''' + a_3 f_i'' + a_4 f_i' + a_5 f_i + b_1 \theta_i + c_1 \phi_i = r_1, \tag{15}$$

$$b_2 \theta_i'' + b_3 \theta_i' + b_4 \theta_i + c_2 \phi_i' = r_2, \tag{16}$$

$$\phi_i'' + c_3 \phi_i' + c_4 f_i + b_5 \theta_i' = r_3, \tag{17}$$

depending on the conditions at the boundary,

$$f_i(0) = f_i'(0) = f_i'(\infty) = \theta_i(0) = \theta_i(\infty) = \phi_i(0) = \phi_i(\infty) = 0,$$

where

$$a_1 = -\beta_2 \sum_{j=0}^{i-1} f_j, a_2 = 1 - \beta_1 (\sum_{j=0}^{i-1} f_j)^2 + 2\beta_2 \sum_{j=0}^{i-1} f_j',$$

$$a_3 = \sum_{j=0}^{i-1} f_j + 2\beta_1 \sum_{j=0}^{i-1} f_j \sum_{j=0}^{i-1} f_j' - 2\beta_2 \sum_{j=0}^{i-1} f_j'',$$

$$a_4 = -2 \sum_{j=0}^{i-1} f_j' + 2\beta_1 \sum_{j=0}^{i-1} f_j \sum_{j=0}^{i-1} f_j'' + 2\beta_2 \sum_{j=0}^{i-1} f_j''' - M,$$

$$a_5 = \sum_{j=0}^{i-1} f_j'' + 2\beta_1 \sum_{j=0}^{i-1} f_j' \sum_{j=0}^{i-1} f_j'' - 2\beta_1 \sum_{j=0}^{i-1} f_j \sum_{j=0}^{i-1} f_j''' - \beta_2 \sum_{j=0}^{i-1} f_j^{iv},$$

$$a_6 = -\sum_{j=0}^{i-1} \theta_j, a_7 = \sum_{j=0}^{i-1} \theta_j', a_8 = -Sc \sum_{j=0}^{i-1} \phi_j, a_9 = -Sc \sum_{j=0}^{i-1} \phi_j',$$

$$b_1 = G_r, b_2 = \left(\frac{1}{Pr}\right) \left(1 + \frac{4}{3} R_d\right), b_3 = \sum_{j=0}^{i-1} f_j, b_4 = -\sum_{j=0}^{i-1} f_j', b_5 = (S_r)(Sc),$$

$$c_1 = G_c, c_2 = D_u, c_3 = Sc \sum_{j=0}^{i-1} f_j, c_4 = -Sc \sum_{j=0}^{i-1} f_j',$$

$$r_1 = \beta_2 \sum_{j=0}^{i-1} f_j \sum_{j=0}^{i-1} f_j^{iv} - \sum_{j=0}^{i-1} f_j''' - \sum_{j=0}^{i-1} f_j \sum_{j=0}^{i-1} f_j'' + \beta_1 \sum_{j=0}^{i-1} f_j''' (\sum_{j=0}^{i-1} f_j)^2 - \\ 2\beta_1 \sum_{j=0}^{i-1} f_j \sum_{j=0}^{i-1} f_j' \sum_{j=0}^{i-1} f_j'' - 2\beta_2 \sum_{j=0}^{i-1} f_j' \sum_{j=0}^{i-1} f_j''' + \beta_2 (\sum_{j=0}^{i-1} f_j'')^2 + (\sum_{j=0}^{i-1} f_j')^2 + M \sum_{j=0}^{i-1} f_j' - \\ G_r \sum_{j=0}^{i-1} \theta_j - G_c \sum_{j=0}^{i-1} \phi_j,$$

$$r_2 = -b_1 \sum_{j=0}^{i-1} \theta_j'' - \sum_{j=0}^{i-1} f_j \sum_{j=0}^{i-1} \theta_j' + \sum_{j=0}^{i-1} f_j' \sum_{j=0}^{i-1} \theta_j - Du \sum_{j=0}^{i-1} \theta_j'',$$

$$r_3 = -\sum_{j=0}^{i-1} \phi_j'' - Sc \sum_{j=0}^{i-1} f_j \sum_{j=0}^{i-1} \phi_j' + Sc \sum_{j=0}^{i-1} f_j' \sum_{j=0}^{i-1} \phi_j - Sc Sr \sum_{j=0}^{i-1} \theta_j''.$$

Using the Chebyshev collocation spectral method [49], the linearized system is solved, producing the following system of equations:

$$\begin{aligned} A_{11} f_i + A_{12} \theta_i + A_{13} \phi_i &= r_1 \\ A_{21} f_i + A_{22} \theta_i + A_{23} \phi_i &= r_2. \\ A_{31} f_i + A_{32} \theta_i + A_{33} \phi_i &= r_3 \end{aligned} \tag{18}$$

We can write system (18) as a matrix equation:

$$A_{i-1} X_i = R_{i-1}, \tag{19}$$

where

$$A_{i-1} = \begin{bmatrix} A_{11} & A_{12} & A_{13} \\ A_{21} & A_{22} & A_{23} \\ A_{31} & A_{32} & A_{33} \end{bmatrix}, X_i = \begin{bmatrix} f_i \\ \theta_i \\ \phi_i \end{bmatrix}, R_{i-1} = \begin{bmatrix} r_1 \\ r_2 \\ r_3 \end{bmatrix},$$

and

$$\begin{aligned} A_{11} &= a_1 D^4 + a_2 D^3 + a_3 D^2 + a_4 D + [a_5], A_{12} = [b_1], A_{13} = [c_1], \\ A_{21} &= a_6 D + [a_7], A_{22} = b_2 D^2 + b_3 D + [b_4], A_{23} = c_2 D^2, \\ A_{31} &= a_8 D + [a_9], A_{32} = b_5 D^2, A_{33} = D^2 + c_3 D + [c_4]. \end{aligned}$$

The resultant system (19) is readily solved as

$$X_i = A_{i-1}^{-1} R_{i-1}. \tag{20}$$

4. Convergence Analysis

The convergence of series solutions to the velocity, temperature, and concentration equations are shown in Table 1. It should be observed that the convergence of $-f''(0)$, $-\theta'(0)$, and $-\phi'(0)$ requires a third-order approximation.

Table 1. Convergence of SLM solutions with respect to several orders of approximations when $Pr = 0.72, Rd = 0.1, \beta_2 = 0.01, Sc = 0.62, Du = 0.03$, and $M = \beta_1 = Sr = Gc = Gr = fw = 0.1$.

Order of Approximation	$-f''(0)$	$-\theta'(0)$	$-\phi'(0)$
1	0.896078971	0.725335707	0.693762086
2	0.896207663	0.725392652	0.693853301
3	0.896207932	0.725392608	0.693853344
4	0.896207932	0.725392608	0.693853344
5	0.896207932	0.725392608	0.693853344
6	0.896207932	0.725392608	0.693853344
10	0.896207932	0.725392608	0.693853344
20	0.896207932	0.725392608	0.693853344
30	0.896207932	0.725392608	0.693853344
40	0.896207932	0.725392608	0.693853344
50	0.896207932	0.725392608	0.693853344

5. Numerical scheme testing

Here, as limiting instances, we verify the accuracy of our numerical results and compare them with the published articles. Thus, we compare the study's results with those reported in references [42],[44], and [50-54]. As Table 2, Table 3, and Table 4 demonstrate, our results are found to be in strong agreement.

Table 2. Comparison of the SLM finding of $-f''(0), -\theta'(0)$, and $-\phi'(0)$ with those found in Khidir and Alsharari [42] for various values of Rd when $Pr = 0.72, \beta_1 = \beta_2 = 0, Sc = 0.62, Du = 0.03, fw = 1$, and $M = Sr = Gc = Gr = 0.1$.

Rd	Ref [42]			Present study		
	$-f''(0)$	$-\theta'(0)$	$-\phi'(0)$	$-f''(0)$	$-\theta'(0)$	$-\phi'(0)$
0.1	0.569474	0.529749	0.514829	0.56936581	0.52969515	0.51467710
0.2	0.568810	0.506361	0.516211	0.56868663	0.50619095	0.51611701
0.5	0.567176	0.450199	0.519572	0.56698916	0.44952390	0.51968217
1.0	0.565239	0.385964	0.523472	0.56491580	0.38411058	0.52393479

Table 3. Comparison of the SLM finding of $-f''(0)$ with those found in [50-53] for various values of β_1 when $\beta_2 = fw = M = Gc = Gr = 0$.

β_1	Ref [50]	Ref [51]	Ref [52]	Ref [53]	Present study
0.0	1.0000	0.99996	0.99996	1.00000	1.000000000
0.2	1.0549	1.05195	1.05195	1.05188	1.051889883
0.4	1.1008	1.10185	1.10185	1.10190	1.101903276
0.6	1.0015	1.15016	1.15016	1.15013	1.150137351
0.8	1.1987	1.19669	1.19669	1.19671	1.196711273

Table 4. Comparison of the SLM finding of $f(\eta)$ with those found in Ghadikolaei et al. [54] and Salah [44] for various values of η when $M = \beta_1 = fw = M = Gc = Gr = 0$.

β_2	η	[54]	[44]	Present
	0	0	0	0
	0.1	0.095199	0.095194	0.095186
	0.2	0.181400	0.181338	0.181357
	0.5	0.394050	0.393892	0.393919
0.01	1	0.633463	0.633460	0.633440
	2	0.866679	0.867642	0.867634
	3	0.952228	0.954211	0.954216
	4	0.983566	0.986229	0.986225
	5	-	0.998059	0.998057

6. Results and Discussion

In this section, we discuss the effect of several relevant parameters on the velocity, temperature, and concentration profiles, which are studied by the plotting of Figs. 1-12. The boundary value problems represented by the nonlinear system of ordinary differential equations (7) - (9) subject to the boundary conditions (10) - (12) were numerically solved using the successive linearization approach. Based on the numerical calculations, Table 5 displays a range of physical parameter values that are significant in this investigation, together with the corresponding local Sherwood number, local Nusselt number, and local skin friction coefficient.

Figure 1 illustrates how the velocity profile is affected by the magnetic field (Hartmann's number, M). Increasing the magnetic field parameter M causes a drop in the velocity profile. We can see that the flow on the profile $f'(\eta)$ diminishes with increasing velocity from a physical

standpoint. This is due to the electrically conductive fluid's reaction to the transverse magnetic field, which produces a Lorentz-type resistance force that tends to restrict the fluid's velocity and motion. According to Figure 2, a strong magnetic force applied results in a high temperature. This is because the Lorentz's force becomes dominant in the strong magnetic field, raising the liquid's temperature as a result. Figure 3 shows how the magnetic parameter M affected the concentration profile as a function of the similarity variable η . The figure shows that the concentration profile $\phi(\eta)$ increases with an increase in the magnetic parameter M .

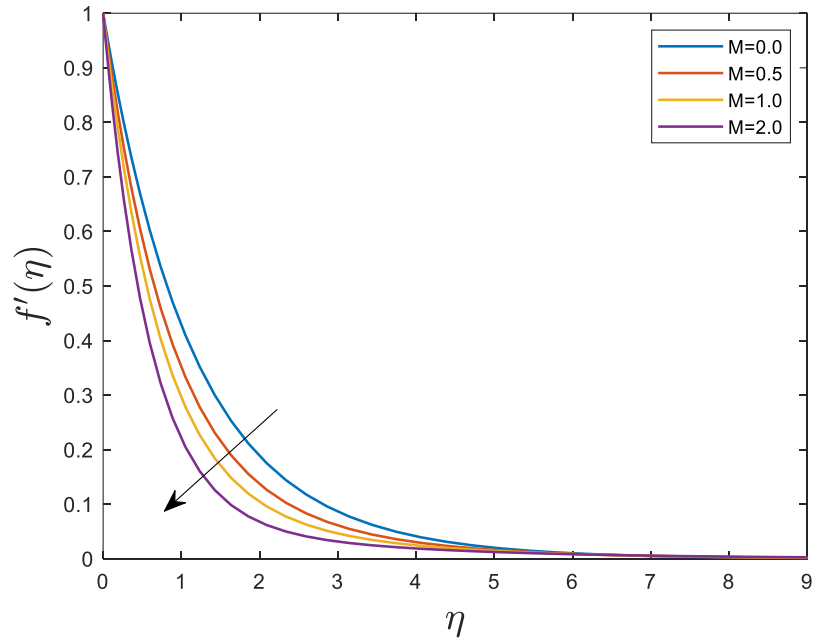


Figure 1. Effect of the magnetic parameter M on the velocity profile.

Table 5. Variations in the local Sherwood number, skin friction coefficient, and Nusselt number for various parameters using SLM when $Pr = 0.72, M = 0.1, \beta_2 = 0.01, Sc = 0.62, Du = 0.03, \text{ and } Rd = \beta_1 = Sr = fw = Gr = Gc = 0.1$.

M	Pr	Rd	β_1	β_2	Sc	Sr	Du	fw	Gr	Gc	$-f''(0)$	$-\theta'(0)$	$-\phi'(0)$
0.0	0.72	0.1	0.1	0.01	0.62	0.1	0.03	0.1	0.1	0.1	0.847757178	0.736421796	0.704778361
0.5											1.073231860	0.685188071	0.654110346
1.0											1.265967555	0.642408855	0.611996545
0.1	0.5	0.1	0.1	0.01	0.62	0.1	0.03	0.1	0.1	0.1	0.889019131	0.578156881	0.706113848
	0.7										0.895668481	0.712946605	0.694827023
	1.0										0.902224993	0.884662431	0.682181805
0.1	0.72	0.0	0.1	0.01	0.62	0.1	0.03	0.1	0.1	0.1	0.898562672	0.782961485	0.689477053
		0.5									0.888594742	0.570553664	0.706795394
		1.0									0.881774463	0.460930692	0.717220792
0.1	0.72	0.1	0.00	0.01	0.62	0.1	0.03	0.1	0.1	0.1	0.881153547	0.731790809	0.700229976
			0.25								0.918095111	0.716258659	0.684772732
			0.50								0.952818124	0.702220948	0.670870011
0.1	0.72	0.1	0.1	0.00	0.62	0.1	0.03	0.1	0.1	0.1	0.899918108	0.724555237	0.693027357
				0.01							0.896207932	0.725392608	0.693853344
				0.02							0.892530082	0.726225967	0.694675505
0.1	0.72	0.1	0.1	0.01	0.5	0.1	0.03	0.1	0.1	0.1	0.891982343	0.729708390	0.607717578
					1.0						0.904862151	0.716433950	0.923268203
					1.5						0.911227332	0.709441823	1.163461832
0.1	0.72	0.1	0.1	0.01	0.62	0.3	0.03	0.1	0.1	0.1	0.893786721	0.727845332	0.638316548
						0.5					0.891402528	0.730227790	0.582655259
						0.7					0.889051446	0.732548813	0.526861351
0.1	0.72	0.1	0.1	0.01	0.62	0.1	0.01	0.1	0.1	0.1	0.896445369	0.730750213	0.693427812
							0.10				0.895379897	0.706604158	0.695337404
							0.30				0.893037964	0.652600769	0.699536846
0.1	0.72	0.1	0.1	0.01	0.62	0.1	0.2	0.0	0.1	0.1	0.950932226	0.751633284	0.717714689
								0.3			0.798392158	0.675889036	0.648782292
								0.5			0.714154777	0.630182126	0.607062204
0.1	0.72	0.1	0.1	0.01	0.62	0.1	0.03	0.1	0.1	0.1	0.896207932	0.725392608	0.693853344
									0.5		0.696899432	0.769118383	0.737166372
									1.0		0.470833902	0.806980260	0.774455176
0.1	0.72	0.1	0.1	0.01	0.62	0.1	0.03	0.1	0.1	0.1	0.896207932	0.725392608	0.693853344
										0.5	0.692792273	0.771096778	0.739171366
										1.0	0.462993477	0.809993478	0.777496971

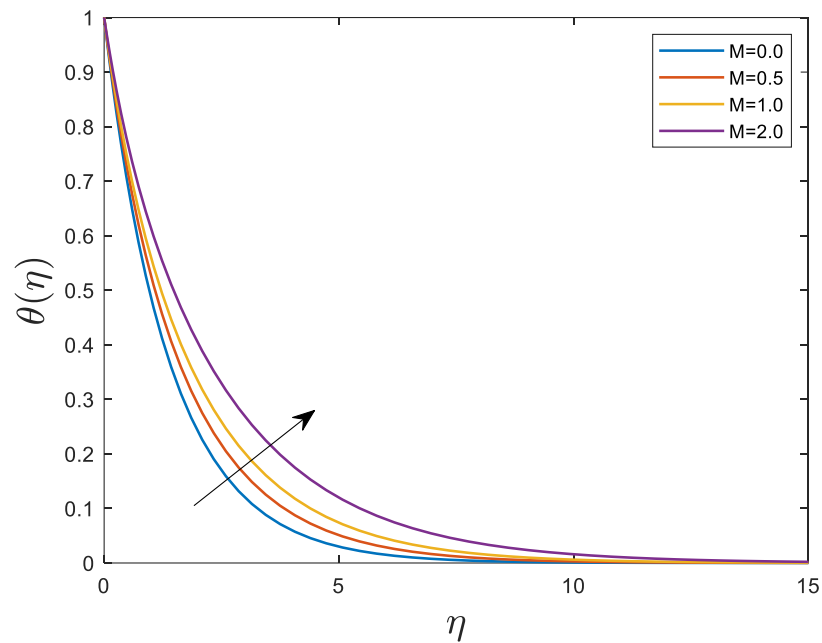


Figure 2. Effect of the magnetic parameter M on the temperature profile.

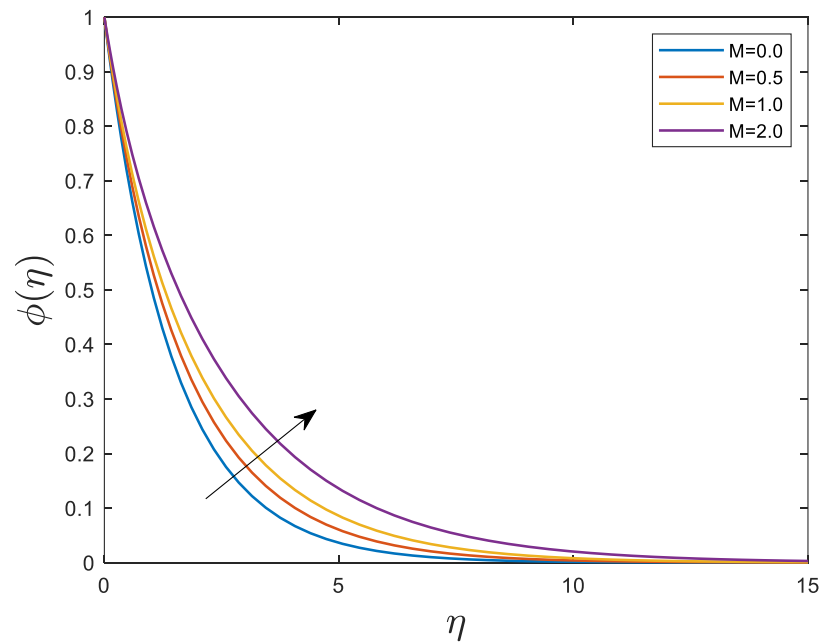


Figure 3. Effect of the magnetic parameter M on the concentration profile.

Figure 4 shows the behavior of the relaxation time constant β_1 on the velocity profile $f'(\eta)$. As the relaxation time constant β_1 increases, a stronger viscous force is created, which restricts the fluid motion and causes the velocity to decrease. Figure 5 shows that the retardation time

constant β_2 has the opposite effect on the velocity field $f'(\eta)$ to the relaxation time constant β_1 . In fact, as the β_2 increases, the viscous forces decrease, and the velocity profile increases.

The effects of the Deborah number β_1 on the temperature profile $\theta(\eta)$ is plotted in Figure 6. Figure 6 shows that using higher Deborah number β_1 values improve the temperature profile $\theta(\eta)$. The Deborah number β_1 is dependent on the amount of time spent relaxing. Higher relaxation times are implied by larger Deborah number β_1 values. It is common knowledge that fluids with longer relaxation times have higher temperatures, whereas those with shorter relaxation times have lower temperatures. Considering this rationale, a larger Deborah number β_1 enhances the temperature profile $\theta(\eta)$.

Figure 7 examines Deborah number β_2 's impact on the dimensionless temperature field. Figure 7 shows that the temperature is a decreasing function of the Deborah number β_2 . In this case, the retardation time affects the Deborah number β_2 . The retardation time increases as we raise the value of the Deborah number β_2 . It is the increase in retardation time that causes the temperature to decrease $\theta(\eta)$. Interestingly, $\beta_1 = 0 = \beta_2$ corresponds to the viscous fluid case in this instance, while $\beta_2 = 0$ illustrates the Maxwell fluid flow scenario.

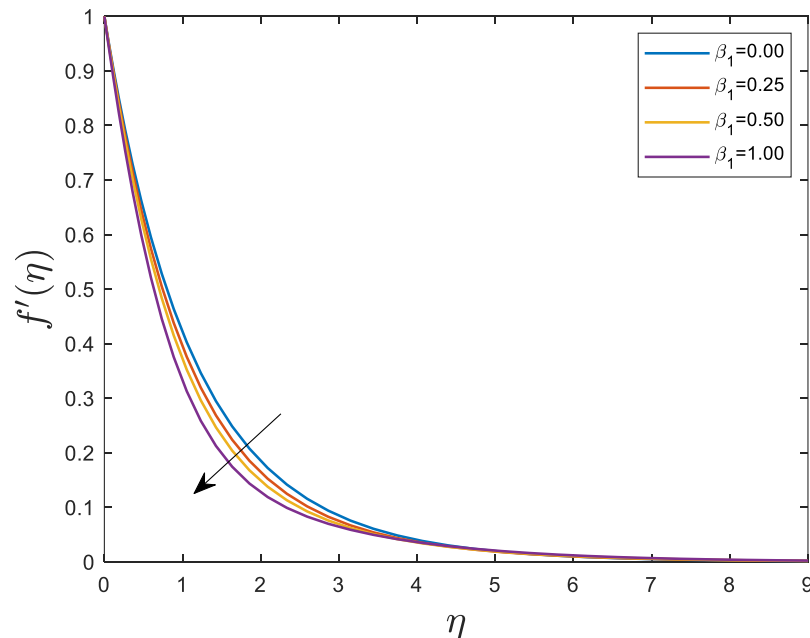


Figure 4. Effect of the Deborah number in terms of the relaxation time β_1 on the velocity profile.

The temperature profile's relationship with the Prandtl number Pr is depicted in Figure 8. Raising the Prandtl numbers results in a decrease in both the temperature and thickness of the thermal layer. There is a physical difference in the thermal diffusivity between larger and smaller Prandtl fluids. A reduced temperature and thermal boundary layer thickness are the results of this shift in thermal diffusivity. The momentum diffusivity divided by the thermal diffusivity is

essentially the Prandtl number. The thermal boundary layer and momentum thicknesses are regulated in heat transmission by the Prandtl number.

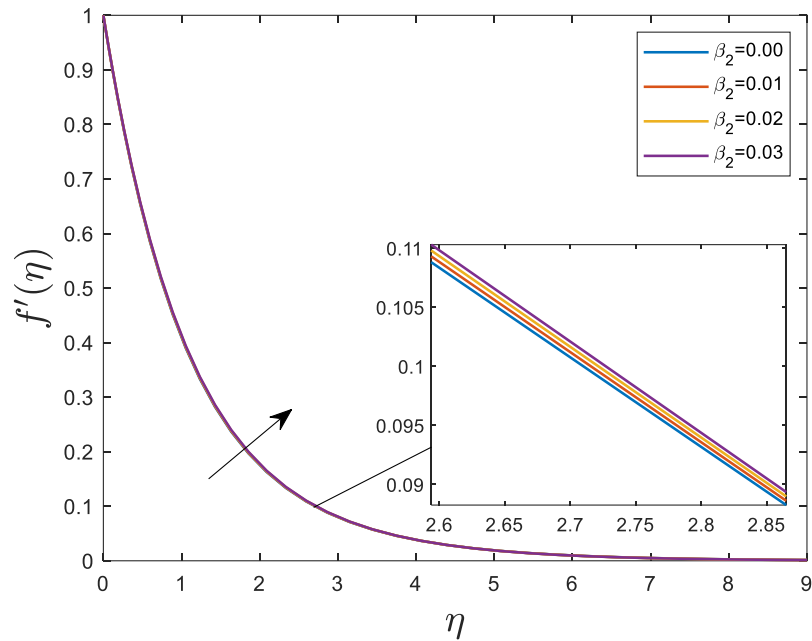


Figure 5. Effect of the Deborah number in terms of the retardation time β_2 on the velocity profile.

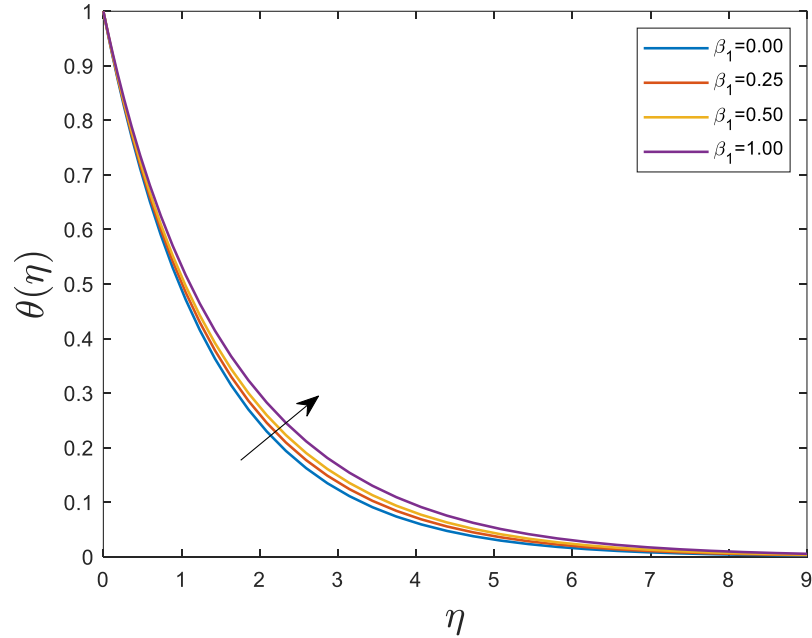


Figure 6. Effect of the Deborah number in terms of the relaxation time β_1 on the temperature profile.

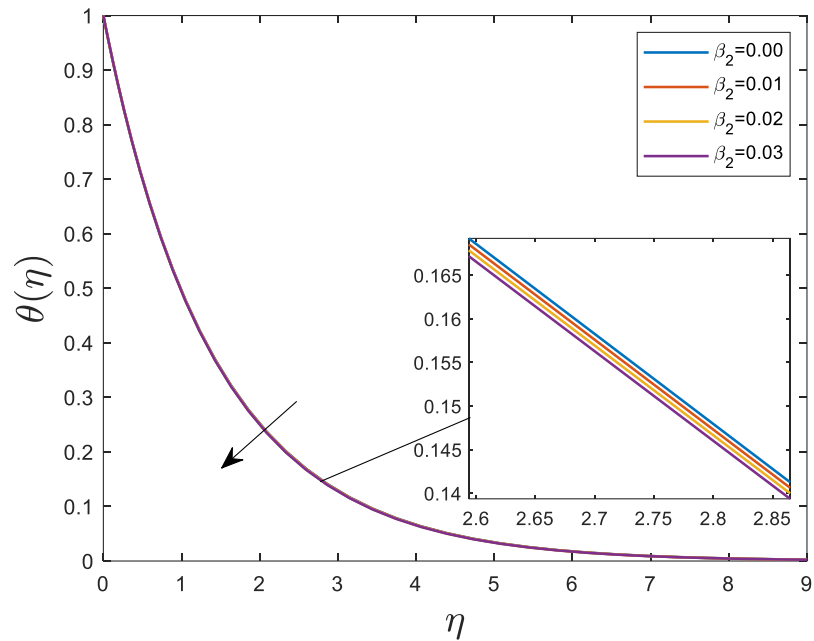


Figure 7. Effect of the Deborah number in terms of the retardation time β_2 on the temperature profile.

Figure 9 illustrates how the thermal radiation parameter Rd affects the temperature profile. As the thermal radiation parameter increases, the temperature and thickness of the thermal boundary layer both rises. Higher thermal radiation parameter values provide the working fluid with more heat, which raises the temperature and thickens the thermal boundary layer.

Figure 10 illustrates the relationship between the temperature and the Dufour number Du . A concentration gradient causes a type of heat flow known as the Dufour effect. When the Dufour effect occurs, the temperature profiles are wider than when it does not. As the thermal boundary layer grows, the boundary layer flow becomes electrified, and the Dufour number increases.

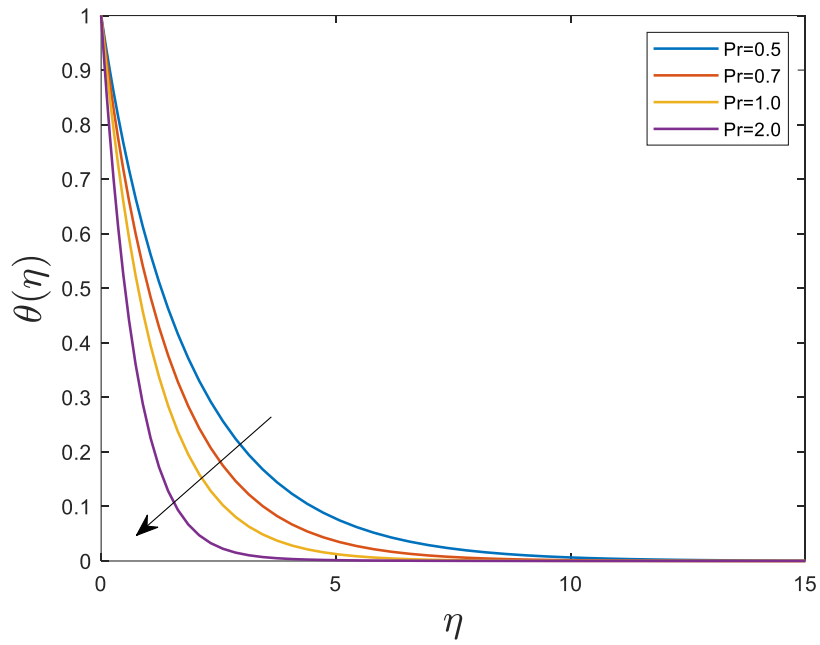


Figure 8. Effect of the Prandtl number Pr on the temperature profile.

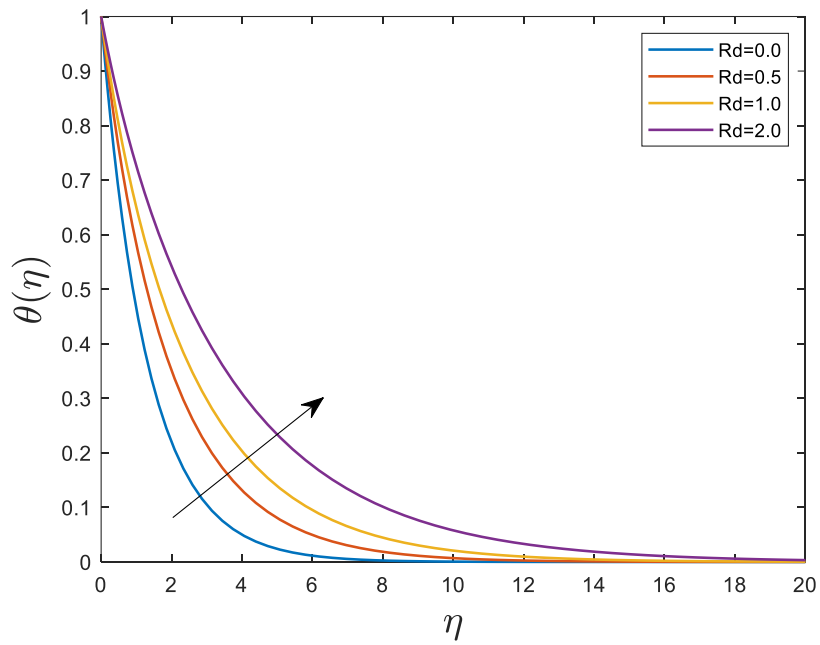


Figure 9. Effect of the thermal radiation parameter Rd on the temperature profile.

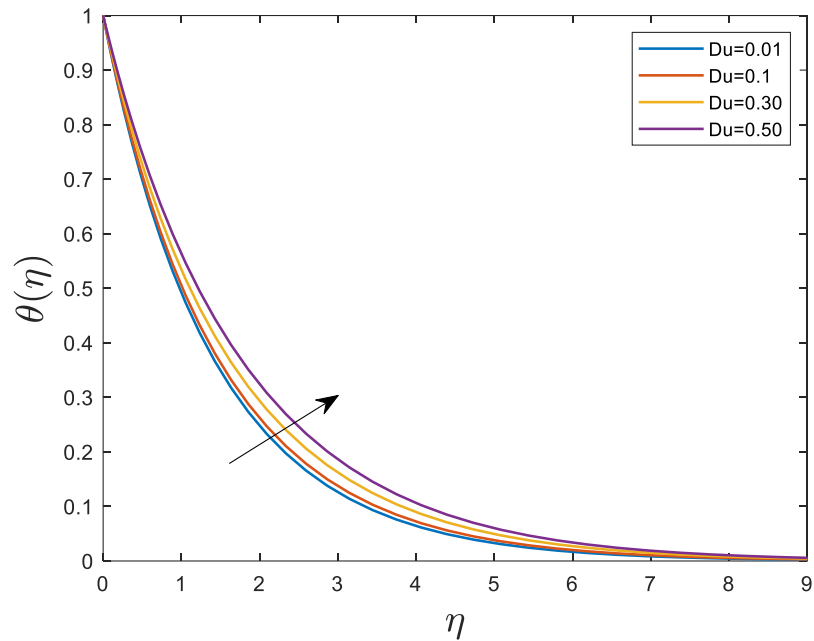


Figure 10. Effect of the Dufour number Du on the temperature profile.

Figure 11 illustrates how the Schmidt number Sc affects the concentration field. It is obvious that the concentration decreases as the Schmidt number increases, as does the thickness of the boundary layer with which it is associated. The Schmidt number and the diffusion coefficient have an inverse relationship. Therefore, a reduced diffusion coefficient is associated with an increase in the Schmidt number. The concentration field is reduced as a result of this decreased diffusion coefficient.

Finally, Figure 12 depicts the increasing nature of the concentration for various estimations of the Soret number Sr . The thermal diffusion (Soret) effect is the term used to describe the mass flux caused by a temperature gradient. It is plausible to infer that as the Soret effect has grown, so has the molar mass's diffusivity, raising the concentration. The Soret effect has enabled isotope separation and gas mixes with low molecular weights.

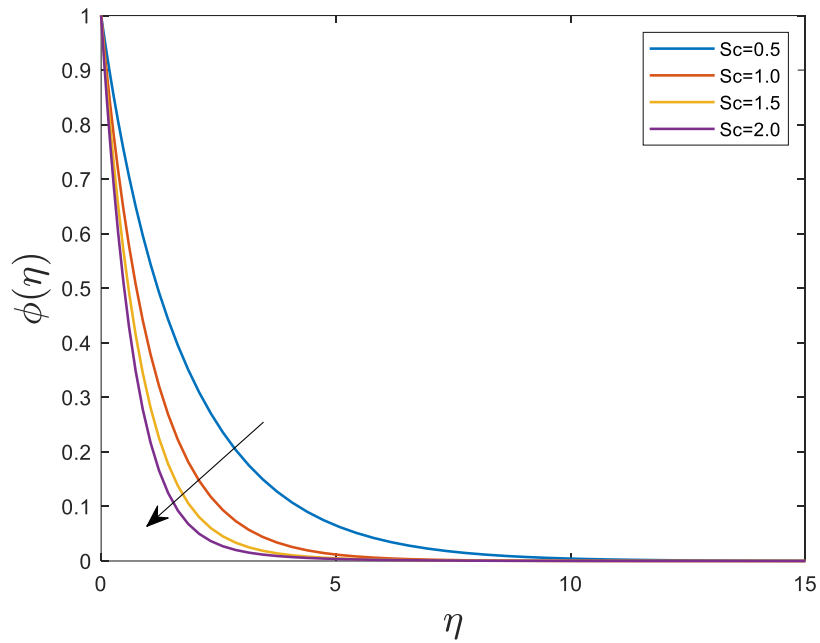


Figure 11. Effect of the Schmidt number Sc on the concentration profile.

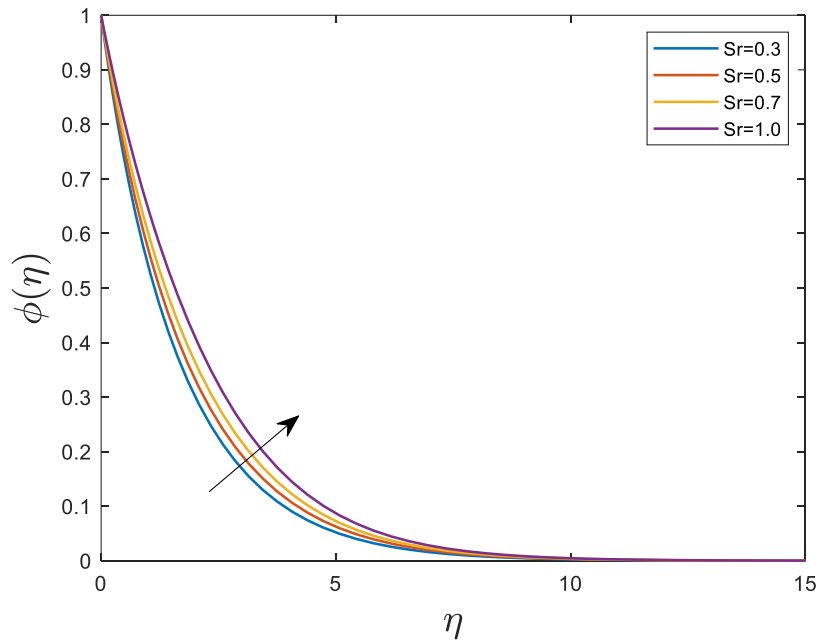


Figure12. Effect of the Soret number Sr on the concentration profile.

Conclusion

The impact of the thermal radiation on the MHD of an Oldroyd-B fluid over a stretching sheet with Soret and Dufour effects was examined. This analysis reduces to the Maxwell fluid, second grad fluid, and viscous fluid flow cases when $\beta_2 = 0$, $\beta_1 = 0$, and $\beta_1 = \beta_2 = 0$ respectively. The main findings of this research are as follows:

- The temperature and concentration components increase, and the velocity profile decreases as the magnetic field increases.
- The concentration component decreases, and the velocity profile temperature distribution increases with increasing radiation parameters.
- Raising the levels of Du and Sr will enhance the temperature and distribution of the concentration.
- Tables 3 and 4 demonstrate the strong consistency, in a limited sense, between our finding and the previously reported.
- It only takes a few iterations to reach the accuracy of the numerical findings, making the SLM very precise, efficient, and fast to converge.

Conflicts of Interest: The author declares that there are no conflicts of interest regarding the publication of this paper.

References

- [1] B. Shilpa, V. Leela, Galerkin Finite Element Analysis of Heat and Mass Transfer of Jeffrey, Maxwell and Oldroyd-B Nanofluids in a Vertical Annulus With an Induced Magnetic Field and a Non-Uniform Heat Source/Sink, *Int. J. Ambient Energy*. 44 (2023), 1887–1903.
<https://doi.org/10.1080/01430750.2023.2196988>.
- [2] B.C. Prasannakumara, M. Gnaneswara Reddy, G.T. Thammanna, B.J. Gireesha, MHD Double-Diffusive Boundary-Layer Flow of a Maxwell Nanofluid Over a Bidirectional Stretching Sheet With Soret and Dufour Effects in the Presence of Radiation, *Nonlinear Eng.* 7 (2018), 195–205.
<https://doi.org/10.1515/nleng-2017-0058>.
- [3] K. Ghachem, A.K. Hussein, L. Kolsi, O. Younis, CNT-Water Nanofluid Magneto-Convective Heat Transfer in a Cubical Cavity Equipped With Perforated Partition, *Eur. Phys. J. Plus*. 136 (2021), 377.
<https://doi.org/10.1140/epjp/s13360-021-01387-y>.
- [4] M. Bhuvaneswari, S. Eswaramoorthi, S. Sivasankaran, A.K. Hussein, Cross-Diffusion Effects on MHD Mixed Convection Over a Stretching Surface in a Porous Medium With Chemical Reaction and Convective Condition, *Eng. Trans.* 67 (2019), 3–19. <https://doi.org/10.24423/engtrans.820.20190308>.
- [5] B. Ali, S.A. Khan, A.K. Hussein, T. Thumma, S. Hussain, Hybrid Nanofluids: Significance of Gravity Modulation, Heat Source/Sink, and Magnetohydrodynamic on Dynamics of Micropolar Fluid Over an Inclined Surface via Finite Element Simulation, *Appl. Math. Comput.* 419 (2022), 126878.
<https://doi.org/10.1016/j.amc.2021.126878>.

- [6] S.E. Ahmed, A.K. Hussein, M.A. Mansour, Z.A. Raizah, X. Zhang, MHD Mixed Convection in Trapezoidal Enclosures Filled With Micropolar Nanofluids, *Nano Sci. Technol. Int. J.* 9 (2018), 343–372. <https://doi.org/10.1615/nanoscitechnolintj.2018026118>.
- [7] J. G. Oldroyd, On the Formulation of Rheological Equations of State, *Proc. R. Soc. Lond. A.* 200 (1950), 523–541. <https://doi.org/10.1098/rspa.1950.0035>.
- [8] T. Hayat, T. Muhammad, S.A. Shehzad, A. Alsaedi, Temperature and Concentration Stratification Effects in Mixed Convection Flow of an Oldroyd-B Fluid with Thermal Radiation and Chemical Reaction, *PLoS ONE.* 10 (2015), e0127646. <https://doi.org/10.1371/journal.pone.0127646>.
- [9] E.S.G. Shaqfeh, Purely Elastic Instabilities in Viscometric Flows, *Annu. Rev. Fluid Mech.* 28 (1996), 129–185. <https://doi.org/10.1146/annurev.fl.28.010196.001021>.
- [10] M. Laso, H.C. Öttinger, Calculation of Viscoelastic Flow Using Molecular Models: The Connffessit Approach, *J. Non-Newtonian Fluid Mech.* 47 (1993), 1–20. [https://doi.org/10.1016/0377-0257\(93\)80042-a](https://doi.org/10.1016/0377-0257(93)80042-a).
- [11] M. Sajid, Z. Abbas, T. Javed, N. Ali, Boundary Layer Flow of an Oldroyd-B Fluid in the Region of a Stagnation Point Over a Stretching Sheet, *Can. J. Phys.* 88 (2010), 635–640. <https://doi.org/10.1139/p10-049>.
- [12] N. Venkatesh, M.A. Kumar, R. Srinivasa Raju, Dufour and Soret Influence on MHD Boundary Layer Flow of a Maxwell Fluid Over a Stretching Sheet With Nanoparticles, *Heat Transfer.* 51 (2022), 5193–5205. <https://doi.org/10.1002/htj.22543>.
- [13] S.S. Motsa, Z.G. Makukula, S. Shateyi, Numerical Investigation of the Effect of Unsteadiness on Three-Dimensional Flow of an Oldroyd-B Fluid, *PLoS ONE.* 10 (2015), e0133507. <https://doi.org/10.1371/journal.pone.0133507>.
- [14] T. Hayat, M. Imtiaz, A. Alsaedi, S. Almezal, On Cattaneo–Christov Heat Flux in MHD Flow of Oldroyd-B Fluid With Homogeneous–Heterogeneous Reactions, *J. Magnetism Magnetic Mater.* 401 (2016), 296–303. <https://doi.org/10.1016/j.jmmm.2015.10.039>.
- [15] K.R. Rajagopal, R.K. Bhatnagar, Exact Solutions for Some Simple Flows of an Oldroyd-B Fluid, *Acta Mech.* 113 (1995), 233–239. <https://doi.org/10.1007/bf01212645>.
- [16] T. Hayat, S.A. Shehzad, A. Alsaedi, M.S. Alhothuali, Three-Dimensional Flow of Oldroyd-B Fluid Over Surface With Convective Boundary Conditions, *Appl. Math. Mech.-Engl. Ed.* 34 (2013), 489–500. <https://doi.org/10.1007/s10483-013-1685-9>.
- [17] T. Hayat, S.A. Shehzad, A. Alsaedi, Three-Dimensional Flow of an Oldroyd-B Fluid Over a Bidirectional Stretching Surface With Prescribed Surface Temperature and Prescribed Surface Heat Flux, *J. Hydrol. Hydromech.* 62 (2014), 117–125. <https://doi.org/10.2478/johh-2014-0016>.
- [18] F. Mabood, G. Bognár, A. Shafiq, Impact of Heat Generation/Absorption of Magnetohydrodynamics Oldroyd-B Fluid Impinging on an Inclined Stretching Sheet With Radiation, *Sci. Rep.* 10 (2020), 17688. <https://doi.org/10.1038/s41598-020-74787-2>.
- [19] B.M. Shankaralingappa, B.C. Prasannakumara, B.J. Giresha, I.E. Sarris, The Impact of Cattaneo–Christov Double Diffusion on Oldroyd-B Fluid Flow over a Stretching Sheet with Thermophoretic Particle Deposition and Relaxation Chemical Reaction, *Inventions.* 6 (2021), 95. <https://doi.org/10.3390/inventions6040095>.

- [20] M. Yasir, A. Ahmed, M. Khan, A.K. Alzahrani, Z.U. Malik, A.M. Alshehri, Mathematical Modelling of Unsteady Oldroyd-B Fluid Flow Due to Stretchable Cylindrical Surface With Energy Transport, *Ain Shams Eng. J.* 14 (2023), 101825. <https://doi.org/10.1016/j.asej.2022.101825>.
- [21] M. Arif, P. Kumam, T. Seangwattana, P. Suttarporn, A Fractional Model Of Magnetohydrodynamics Oldroyd-B Fluid With Couple Stresses, Heat and Mass Transfer: A Comparison Among Non-Newtonian Fluid Models, *Heliyon.* 9 (2023), e17642. <https://doi.org/10.1016/j.heliyon.2023.e17642>.
- [22] P.V. Satya Narayana, B. Venkateswarlu, Soret and Dufour Effects on Mhd Flow of a Maxwell Fluid Over a Stretching Sheet With Joule Heating, *Front. Heat Mass Transfer.* 9 (2017), 11. <https://doi.org/10.5098/hmt.9.11>.
- [23] T. Hayat, S.A. Shehzad, A. Alsaedi, Soret and Dufour Effects on Magnetohydrodynamic (MHD) Flow of Casson Fluid, *Appl. Math. Mech.-Engl. Ed.* 33 (2012), 1301–1312. <https://doi.org/10.1007/s10483-012-1623-6>.
- [24] S.A. Khan, T. Hayat, A. Alsaedi, Simultaneous Features of Soret And Dufour in Entropy Optimized Flow of Reiner-Rivlin Fluid Considering Thermal Radiation, *Int. Commun. Heat Mass Transfer.* 137 (2022), 106297. <https://doi.org/10.1016/j.icheatmasstransfer.2022.106297>.
- [25] M.M. Biswal, K. Swain, G.C. Dash, K. Ojha, Study of Radiative Magneto-Non-Newtonian Fluid Flow Over a Nonlinearly Elongating Sheet With Soret and Dufour Effects, *Numer. Heat Transfer, Part A: Appl.* 83 (2022), 331–342. <https://doi.org/10.1080/10407782.2022.2091379>.
- [26] N.K. Mishra, M. Sharma, B.K. Sharma, U. Khanduri, Soret and Dufour Effects on MHD Nanofluid Flow of Blood Through a Stenosed Artery With Variable Viscosity, *Int. J. Mod. Phys. B.* 37 (2023), 2350266. <https://doi.org/10.1142/s0217979223502661>.
- [27] X. Yang, Y. Zhang, Lattice Boltzmann Study of the Double-Diffusive Convection in Porous Media With Soret and Dufour Effects, *Comput. Geosci.* (2023). <https://doi.org/10.1007/s10596-023-10251-0>.
- [28] N. Vijay, K. Sharma, Magnetohydrodynamic Hybrid Nanofluid Flow Over a Decelerating Rotating Disk With Soret and Dufour Effects, *Multidiscip. Model. Mater. Struct.* 19 (2023), 253–276. <https://doi.org/10.1108/mmms-08-2022-0160>.
- [29] S.A. Khan, T. Hayat, A. Alsaedi, Numerical Study for Entropy Optimized Radiative Unsteady Flow of Prandtl Liquid, *Fuel.* 319 (2022), 123601. <https://doi.org/10.1016/j.fuel.2022.123601>.
- [30] M. Jawad, A. Saeed, A. Khan, I. Ali, H. Alrabaiah, T. Gul, E. Bonyah, M. Zubair, Analytical Study of MHD Mixed Convection Flow for Maxwell Nanofluid With Variable Thermal Conductivity and Soret and Dufour Effects, *AIP Adv.* 11 (2021), 035215. <https://doi.org/10.1063/5.0029105>.
- [31] M.V. Reddy, P. Lakshminarayana, K. Vajravelu, Magnetohydrodynamic Radiative Flow of a Maxwell Fluid on an Expanding Surface With the Effects of Dufour and Soret and Chemical Reaction, *Comput. Therm. Sci.* 12 (2020), 317–327. <https://doi.org/10.1615/computthermalsci.2020034147>.
- [32] S. Liao, *Beyond Perturbation: Introduction to the Homotopy Analysis Method*, CRC Press, 2003.
- [33] O.D. Makinde, Effect of Arbitrary Magnetic Reynolds Number on MHD Flows in Convergent-Divergent Channels, *Int. J. Numer. Methods Heat Fluid Flow.* 18 (2008), 697–707. <https://doi.org/10.1108/09615530810885524>.
- [34] Z. Makukula, On a New Solution for the Viscoelastic Squeezing Flow between Two Parallel Plates, *J. Adv. Res. Appl. Math.* 2 (2010), 31–38. <https://doi.org/10.5373/jaram.455.060310>.

- [35] Z.G. Makukula, P. Sibanda, S.S. Motsa, A Novel Numerical Technique for Two-Dimensional Laminar Flow between Two Moving Porous Walls, *Math. Probl. Eng.* 2010 (2010), 528956. <https://doi.org/10.1155/2010/528956>.
- [36] M. Narayana, P. Sibanda, On the Solution of Double-Diffusive Convective Flow due to a Cone by a Linearization Method, *J. Appl. Math.* 2012 (2012), 587357. <https://doi.org/10.1155/2012/587357>.
- [37] S. Shateyi, S. Motsa, Variable Viscosity on Magnetohydrodynamic Fluid Flow and Heat Transfer over an Unsteady Stretching Surface with Hall Effect, *Bound Value Probl.* 2010 (2010), 257568. <https://doi.org/10.1155/2010/257568>.
- [38] M. A. Mohammed Ahmed, M.E. Mohammed, A.A. Khidir, On Linearization Method to MHD Boundary Layer Convective Heat Transfer With Low Pressure Gradient, *Propuls. Power Res.* 4 (2015), 105–113. <https://doi.org/10.1016/j.jprr.2015.04.001>.
- [39] A.A. Khidir, Application of Successive Linearisation Method on Mixed Convection Boundary Layer Flow of Nanofluid from an Exponentially Stretching Surface with Magnetic Field Effect, *J. Nanofluids.* 12 (2023), 465–475. <https://doi.org/10.1166/jon.2023.1961>.
- [40] Y. Daoud, M. Abdalbagi, A.A. Khidir, On the Solution of Magneto-Hydrodynamics Three-Dimensional Flow Due to a Stretching Sheet in a Porous Medium Using the Successive Linearization Method, *Chinese J. Phys.* 73 (2021), 232–238. <https://doi.org/10.1016/j.cjph.2021.06.011>.
- [41] F. Salah, A.K. Alzahrani, A. O. Sidahmed, K.K. Viswanathan, A Note on Thin-Film Flow of Eyring-Powell Fluid on the Vertically Moving Belt Using Successive Linearization Method, *Int. J. Adv. Appl. Sci.* 6 (2019), 17–22. <https://doi.org/10.21833/ijaas.2019.02.004>.
- [42] A.A. Khidir, S.L. Alsharari, Application of Successive Linearisation Method on the Boundary Layer Flow Problem of Heat and Mass Transfer with Radiation Effect, *Int. J. Anal. Appl.* 19 (5) (2021), 725–742. <https://doi.org/10.28924/2291-8639-19-2021-725>.
- [43] R. Cortell, A Note on Flow And Heat Transfer of a Viscoelastic Fluid Over a Stretching Sheet, *Int. J. Non-Linear Mech.* 41 (2006), 78–85. <https://doi.org/10.1016/j.ijnonlinmec.2005.04.008>.
- [44] F. Salah, Numerical Solution for Heat Transfer of Oldroyd-B Fluid Over a Stretching Sheet Using Successive Linearization Method, *Int. J. Adv. Appl. Sci.* 7 (2020), 40–47. <https://doi.org/10.21833/ijaas.2020.06.006>.
- [45] Z. Makukula, P. Sibanda, S. Motsa, A Note on the Solution of the Von Kármán Equations Using Series and Chebyshev Spectral Methods, *Bound Value Probl.* 2010 (2010), 471793. <https://doi.org/10.1155/2010/471793>.
- [46] M.A. Mohammed Ahmed, M.E. Mohammed, A.A. Khidir, The Effects of Cross-Diffusion and Radiation on Mixed Convection From a Vertical Flat Plate Embedded in a Fluid-Saturated Porous Medium in the Presence of Viscous Dissipation, *Propuls. Power Res.* 5 (2016), 149–163. <https://doi.org/10.1016/j.jprr.2016.05.001>.
- [47] A. Sidahmed, F. Salah, Radiation Effects on MHD Flow of Second Grade Fluid Through Porous Medium Past an Exponentially Stretching Sheet With Chemical Reaction, *J. Adv. Res. Fluid Mech. Therm. Sci.* 99 (2022), 1–16. <https://doi.org/10.37934/arfmts.99.2.116>.

- [48] F. Salah, M.H. Elhafian, Numerical Solution for Heat Transfer of Non-Newtonian Second-Grade Fluid Flow over Stretching Sheet via Successive Linearization Method, *IAENG Int. J. Appl. Math.* 49 (2019), 505.
- [49] M.Y. Hussaini, T.A. Zang, Spectral Methods in Fluid Dynamics, *Ann. Rev. Fluid Mech.* 19 (1987), 339–367. <https://doi.org/10.1146/annurev.fl.19.010187.002011>.
- [50] K. Sadeghy, H. Hajibeygi, S.-M. Taghavi, Stagnation-Point Flow of Upper-Convected Maxwell Fluids, *Int. J. Non-Linear Mech.* 41 (2006), 1242–1247. <https://doi.org/10.1016/j.ijnonlinmec.2006.08.005>.
- [51] M. Subhas Abel, J.V. Tawade, M.M. Nandeppanavar, MHD Flow and Heat Transfer for the Upper-Convected Maxwell Fluid Over a Stretching Sheet, *Meccanica.* 47 (2011), 385–393. <https://doi.org/10.1007/s11012-011-9448-7>.
- [52] M.S. Mandal, S. Mukhopadhyay, The Flow of MHD Maxwell Liquid Over an Extending Surface With Variable Free Stream Temperature, *Heat Trans.* 51 (2022), 6801–6814. <https://doi.org/10.1002/htj.22624>.
- [53] M. Waqas, T. Hayat, S.A. Shehzad, A. Alsaedi, Transport of Magneto hydrodynamic Nanomaterial in a Stratified Medium Considering Gyrotactic Microorganisms, *Physica B: Condensed Matter.* 529 (2018), 33–40. <https://doi.org/10.1016/j.physb.2017.09.128>.
- [54] S.S. Ghadikolaei, Kh. Hosseinzadeh, M. Yassari, H. Sadeghi, D.D. Ganji, Analytical and Numerical Solution of Non-Newtonian Second-Grade Fluid Flow on a Stretching Sheet, *Therm. Sci. Eng. Progress.* 5 (2018), 309–316. <https://doi.org/10.1016/j.tsep.2017.12.010>.